also can be applied to TEGO (figs. S11 and S12), which is already being manufactured in ton quantities (*13*). By use of this type of simple activation process already commercially demonstrated for ACs, scaled a-MEGO and a-TEGO production for advanced energy/power electrochemical electrical energy storage devices may be realized in a short period.

References and Notes

1. J. R. Miller, P. Simon, *Science* **321**, 651 (2008).
2. A. Burke, *Electrochim. Acta* **53**, 1083 (2007).
3. J. A. Fernandez *et al*., *J. Power Sources* **175**, 675 (2008).
4. P. Simon, Y. Gogotsi, *Nat. Mater.* **7**, 845 (2008).
5. J. Chmiola *et al*., *Science* **313**, 1760 (2006).
6. N. L. Wu, *Mater. Chem. Phys.* **75**, 6 (2002).
7. T. Brezesinski, J. Wang, S. H. Tolbert, B. Dunn, *Nat. Mater.* **9**, 146 (2010).
8. A. Rudge, J. Davey, I. Raistrick, S. Gottesfeld, J. P. Ferraris, *J. Power Sources* **47**, 89 (1994).
9. M. Toupin, T. Brousse, D. Belanger, *Chem. Mater.* **16**, 3184 (2004).
10. A. Izadi-Najafabadi *et al*., *Adv. Mater.* **22**, E235 (2010).
11. D. N. Futaba *et al*., *Nat. Mater.* **5**, 987 (2006).
12. Y. Zhu *et al*., *Adv. Mater.* **22**, 3906 (2010).
13. M. Segal, *Nat. Nanotechnol.* **4**, 612 (2009).
14. M. D. Stoller, S. J. Park, Y. W. Zhu, J. H. An, R. S. Ruoff, *Nano Lett.* **8**, 3498 (2008).
15. Y. Wang *et al*., *J. Phys. Chem. C* **113**, 13103 (2009).
16. W. Lv *et al*., *ACS Nano* **3**, 3730 (2009).
17. Y. Zhu *et al*., *ACS Nano* **4**, 1227 (2010).
18. S. R. C. Vivekchand, C. S. Rout, K. S. Subrahmanyam, A. Govindaraj, C. N. R. Rao, *J. Chem. Sci.* **120**, 9 (2008).
19. J. R. Miller, R. A. Outlaw, B. C. Holloway, *Science* **329**, 1637 (2010).
20. Y. Zhu *et al*., *Carbon* **48**, 2118 (2010).
21. H. Marsh, F. Rodriguez-Reinoso, *Activated Carbon*. (Elsevier, London, 2006).
22. E. Raymundo-Pinero *et al*., *Carbon* **43**, 786 (2005).
23. V. Barranco *et al*., *J. Phys. Chem. C* **114**, 10302 (2010).
24. T. Liu, T. V. Sreekumar, S. Kumar, R. H. Hauge, R. E. Smalley, *Carbon* **41**, 2440 (2003).
25. M. A. Lillo-Rodenas, D. Cazorla-Amoros, A. Linares-Solano, *Carbon* **41**, 267 (2003).
26. J. A. Leiro, M. H. Heinonen, T. Laiho, I. G. Batirev, *J. Electron Spectrosc. Relat. Phenom.* **128**, 205 (2003).
27. S. D. Berger, D. R. McKenzie, P. J. Martin, *Philos. Mag. Lett.* **57**, 285 (1988).
28. P. I. Ravikovitch, A. Vishnyakov, R. Russo, A. V. Neimark, *Langmuir* **16**, 2311 (2000).
29. K. S. W. Sing *et al*., *Pure Appl. Chem.* **57**, 603 (1985).
30. J. C. Groen, L. A. A. Peffer, J. Perez-Ramirez, *Microporous Mesoporous Mater.* **60**, 1 (2003).
31. A. V. Neimark, Y. Lin, P. I. Ravikovitch, M. Thommes, *Carbon* **47**, 1617 (2009).
32. M. D. Stoller, R. S. Ruoff, *Energy Environ. Sci.* **3**, 1294 (2010).
33. P. L. Taberna, P. Simon, J. F. Fauvarque, *J. Electrochem. Soc.* **150**, A292 (2003).
34. C. Portet, M. A. Lillo-Ródenas, A. Linares-Solano, Y. Gogotsi, *Phys. Chem. Chem. Phys.* **11**, 4943 (2009).
35. C. O. Ania, J. Pernak, F. Stefaniak, E. Raymundo-Pinero, F. Beguin, *Carbon* **44**, 3126 (2006).
36. C. Largeot *et al*., *J. Am. Chem. Soc.* **130**, 2730 (2008).
37. S. J. Townsend, T. J. Lenosky, D. A. Muller, C. S. Nichols, V. Elser V, *Phys. Rev. Lett.* **69**, 921 (1992).
38. H. Terrones, A. L. Mackay, *Prog. Cryst. Growth Charact. Mater.* **34**, 25 (1997).
39. E. Barborini *et al*., *Appl. Phys. Lett.* **81**, 3359 (2002).

Acknowledgments: We appreciate funding support from NSF under award DMR-0907324, the U.S. Department of Energy (DOE) under award DE-SC001951, and the Institute for Advanced Technology. The research by E.A. and D.S. has been carried out at the Center for Functional Nanomaterials, Brookhaven National Laboratory, which is supported by the DOE, Office of Basic Energy Sciences, under contract DE-AC02-98CH10886. We thank P. Stephens for XRD data collection, which is supported by DOE under contract DE-AC02-98CH10886, and P. Ercius for data collection on the TEAM instrument, supported by DOE contract DE-AC02-05CH11231. We thank M. Nilges for help with EPR. We thank J. Potts for providing graphite oxide samples. We appreciate use of equipment in K. Johnston's lab. R.M.W. and A.P. acknowledge the partial support of the GRC-NRI SWAN Center for the XPS data collection and analysis. R.S.R., Y.Z., M.D.S., and S.M. have filed a U.S. patent application (application no. PCT/US2011/036164) regarding work in this paper.

Supporting Online Material

www.sciencemag.org/cgi/content/full/science.1200770/DC1
SOM Text
Figs. S1 to S12
References
Movie S1

22 November 2010; accepted 2 May 2011
Published online 12 May 2011;
10.1126/science.1200770

Disorder-Enhanced Transport in Photonic Quasicrystals

Liad Levi,* Mikael Rechtsman,* Barak Freedman, Tal Schwartz, Ofer Manela, Mordechai Segev†

Quasicrystals are aperiodic structures with rotational symmetries forbidden to conventional periodic crystals; examples of quasicrystals can be found in aluminum alloys, polymers, and even ancient Islamic art. Here, we present direct experimental observation of disorder-enhanced wave transport in quasicrystals, which contrasts directly with the characteristic suppression of transport by disorder. Our experiments are carried out in photonic quasicrystals, where we find that increasing disorder leads to enhanced expansion of the beam propagating through the medium. By further increasing the disorder, we observe that the beam progresses through a regime of diffusive-like transport until it finally transitions to Anderson localization and the suppression of transport. We study this fundamental phenomenon and elucidate its origins by relating it to the basic properties of quasicrystalline media in the presence of disorder.

Anderson localization (*1*), a fundamental concept in solid-state physics, describes how introducing disorder can transform a conducting crystal into an insulator. This prediction and subsequent experiments have shown that, generally, disorder works to arrest transport in periodic systems containing disorder (*2*–*5*), as well as in fully random potentials (*6*–*10*). However, some systems still pose fundamental challenges to this concept—most notably, quasicrystals. Quasicrystals (QCs) (*11*, *12*) constitute an intermediate phase between fully periodic and fully disordered media: They do not have a unit cell and do not exhibit translation symmetry; nevertheless, they possess noncrystallographic rotational symmetry and long-range order and display Bragg diffraction. Although many of the properties of QCs are now well understood, some fundamental questions remain. Perhaps one of the most intriguing questions related to QCs has to do with transport. Opposite to crystals containing disorder, which exhibit Anderson localization, it has been suggested that disorder can enhance transport in QCs (*13*, *14*). Indirect experiments have indicated that in some regimes, increasing disorder could enhance transport (*14*).

The electronic structure of atomic QCs has been shown to have multifractal eigenstates (*15*, *16*), which may or may not be normalizable (thus, localized), depending on the critical exponent associated with the given state. The transport properties of QCs are directly related to the critical nature of their eigenstates, in particular, in the presence of disorder (*17*). QCs have been shown to exhibit counterintuitive transport properties, including extremely low conductivity that increases with both temperature (inverse Matheisen rule) and spatial disorder arising from structural defects (*14*). Both of these effects have been attributed (*16*, *18*) to hopping between critical states of different spatial extents near the Fermi energy (due to inelastic electron-phonon scattering for the former and elastic scattering from structural defects for the latter). This increase in transport with disorder is directly opposite to the characteristic behavior of crystals, wherein transport is reduced with increasing disorder.

Thus far, experiments on transport in atomic QCs were carried out by the study of macroscopic conductivity. However, conductivity experiments are problematic for addressing some basic questions on QCs. First, the mechanisms proposed to explain the unusual transport in QCs assume noninteracting electrons; however, conductivity measurements inevitably incorporate electron-electron interactions. Second, conductivity measurements do not allow direct observation of wave packets, which could be a key property in unraveling the mechanisms underlying transport. With the recent progress in photonic lattices (*19*), manifesting analogies between light propagating in a waveguide

Department of Physics and Solid State Institute, Technion, Haifa 32000, Israel.

*These authors contributed equally to this work.
†To whom correspondence should be addressed. E-mail: msegev@tx.technion.ac.il

array and an electron in an atomic lattice, it is natural to expect experimental studies of transport in photonic QCs. Indeed, experiments have studied the QC band structure (*20*), the dynamics of phasons (*21*), and propagation though QCs without disorder (*22*, *23*). However, the fundamental issue of transport in photonic QCs in the presence of disorder has not previously been studied experimentally.

Here, we study photonic quasicrystals containing disorder and present the first direct experimental observation of disorder-enhanced transport in QCs by directly imaging wave packets propagating through the photonic QC containing disorder. We show that disorder considerably enhances the transport of wave packets associated with eigenstates in the proximity of a pseudogap (a sharp reduction in the density of states), the region in which the Fermi energy is found in electronic systems. Enhanced transport occurs because disorder acts to couple highly localized states near the pseudogap, and as a result, states become more extended. When disorder is further increased, we experimentally demonstrate finite-time, diffusive-like transport, as predicted for weakly disordered QCs (*24*). Upon increasing the disorder even further, Anderson localization prevails: the width of the wave packet shrinks, and its tails display exponential decay. Our photonic system is equivalent to a two-dimensional (2D) Penrose QC containing disorder, and the wave packet we image is analogous to the probability amplitude of an electron propagating in it; hence, our findings are relevant to conduction electrons in quasicrystalline electronic systems.

We work with photonic lattices, in the transverse localization scheme (*25*), described by the paraxial equation for monochromatic light

$$i\frac{\partial \Psi}{\partial z} = \hat{H}\Psi \triangleq \left[-\frac{1}{2k}\left(\frac{\partial^2}{\partial x^2}+\frac{\partial^2}{\partial y^2}\right)-\frac{k}{n_0}\Delta n(x,y)\right]\Psi \quad (1)$$

Here z is the propagation coordinate, x and y are the transverse coordinates, $\hat{H}$ is the Hamiltonian (defined by Eq. 1), Ψ is the slowly varying envelope of an optical field $E(x,y,z,t) = \mathrm{Re}[\Psi(x,y,z)e^{i(kz-\omega t)}]$ (t is the time coordinate) of frequency ω and wave number $k = \omega n_0/c$, n_0 is the bulk refractive index, Δn is the local change in the refractive index (lattice plus disorder), and $i^2 = -1$. Equation 1 has the form of the Schrödinger equation: the equivalence emerges when $z \rightarrow t$ and $-\Delta n \rightarrow V$ (where V is the potential). Hence, the evolution of a light beam behaves like the wave packet of a quantum particle in a 2D potential, but with the coordinate z replacing time. Solving for the eigenstates $\Psi_\beta = A_\beta(x,y)\exp(-i\beta z)$ (A_β is the z-independent eigenmode), for which $\hat{H}\Psi_\beta = \beta\Psi_\beta$ (β is the energy), is the equivalent to solving for the eigenmode of a particle, where the propagation constant corresponds to the eigenenergy E. Our photonic QC containing disorder is a Penrose-tiled 2D refractive index structure on which we superimpose 2D random disorder. The refractive index structure $\Delta n(x,y)$ corresponds to an array of parallel waveguides, ordered as a Penrose tiling, with random transverse variations whose strength is controlled at will.

Figure 1 shows the experimental scheme. We use the induction technique (*26*) to transform an optical intensity pattern into a z-independent refractive index structure $\Delta n(x,y,z)$, which includes both the QC lattice and the disorder (*27*). We study transport by launching a weak probe beam and monitoring the beam exiting the sample (*28*). Meaningful results are obtained by repeating experiments multiple times with many realizations of the disorder (same parameters) and ensemble-averaging over the intensity patterns at the exit face.

We now describe the results on enhanced transport in disordered QCs. The simulation results, shown in Fig. 2A, display the ensemble-averaged width, W_{eff} (*3*, *29*), of the beam propagating through the QC, without disorder (lower curve) and with 20% disorder (upper curve). We numerically launch a narrow Gaussian beam at a center of local 10-fold symmetry in the QC structure (center of a "flower"; see two example points marked by arrows in Fig. 2B). Without disorder, transport through the pure QC displays a "bumpy ride," with irregular oscillations occurring because of the presence of states of very different spatial extent within small energy ranges. On the other hand, transport through the QC containing disorder is considerably enhanced (Fig. 2A, upper curve): Throughout propagation, the width of the beam propagating in the disordered QC is larger than the width of the beam propagating in the pure QC. Moving the launch point to any

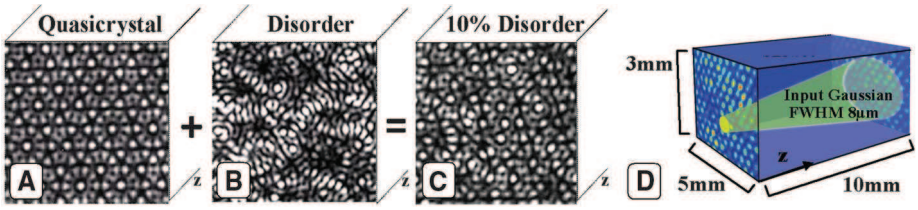

Fig. 1. Experimental scheme for transverse localization in photonic QCs containing disorder. A narrow optical beam is launched at the input face of a 2D quasicrystal lattice (**A**) containing disorder (**B** and **C**). The output intensity (**D**) pattern is monitored and ensemble-averaged over many realizations of disorder. FWHM, full width at half maximum.

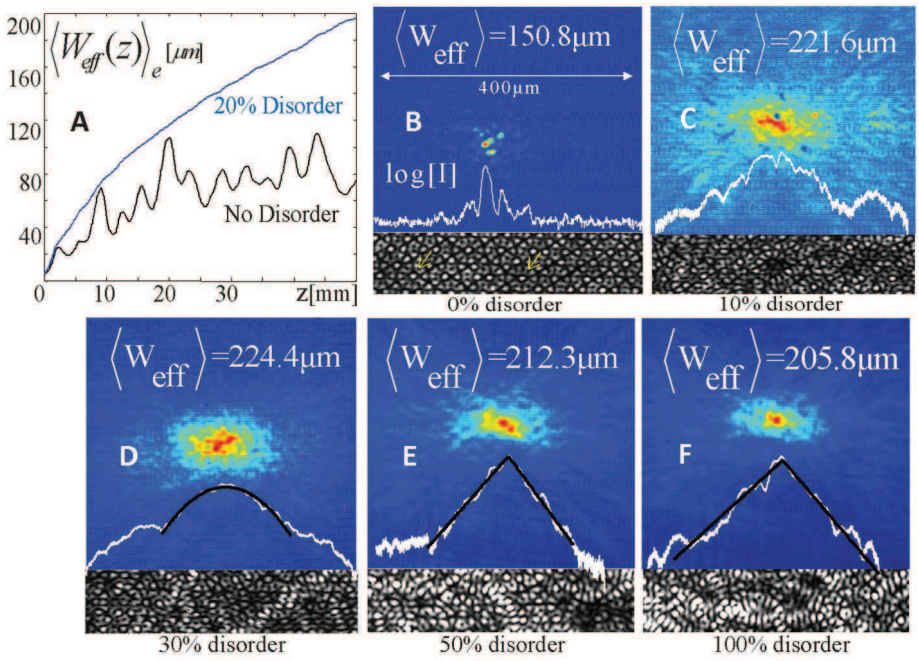

Fig. 2. Experimental and simulation results of transport through photonic quasicrystals, demonstrating disorder-enhanced transport and Anderson localization. (**A**) Simulation: beam width (ensemble-averaged) versus propagation distance for a pure QC (black) and a QC containing 20% disorder (blue). Transport is always higher in the disordered QC. (**B** to **F**) Experimental results: output intensity after z = 10 mm (ensemble-averaged), the log of its cross section (shown in white), and samples of the refractive-index profile (below each panel). Disorder-enhanced transport is apparent from the transition from 0% to 10% disorder [(B) and (C)]. For higher disorder levels, parabolic and linear fits [in (D) to (F)] indicate diffusive-like transport and the transition to Anderson localization, respectively. Yellow arrows in (B) indicate points of local 10-fold symmetry.

other center of local 10-fold symmetry yields virtually identical results. The experimental results are depicted in Fig. 2, B to F. Figure 2B shows the beam exiting the pure QC after 10 mm of propagation. The exiting beam, which has a mean width (W_{eff}) of ~150 μm, is always fractured and varies depending on the launch point, because the QC has no translational symmetry. Figure 2, C to F, depicts the ensemble-averaged output beam and its log-plot cross section, for increasing strength of disorder. The ensemble averaging is taken over 100 realizations of the disorder for Fig. 2, B to D, and over 50 realizations for Fig. 2, E and F, for each value of disorder strength. At 30% disorder (Fig. 2D), the wave packet is diffusive-like, as indicated by the parabolic cross section near the center of (the log of) the ensemble-averaged beam. A parabolic fit to these data in the central region, where the signal is strongest, gives a R^2 goodness-of-fit value of 96% (as shown in the figure). Notice that the width of the averaged beam in Fig. 2, C and D (221.6 and 224.4 μm, with standard deviations of 47 and 31 μm, respectively) is greater than the width of the output beam in the pure QC (150.8 mm in Fig. 2A), indicating enhanced transport. On the other hand, further increasing the disorder strength (50 and 100% disorder) makes the beam more localized (Fig. 2, E and F), while displaying the exponential tails characteristic of the transition to Anderson localization, with an average beam width of 212 and 206 μm (standard deviations of 28 and 35 μm), respectively. The linear fits to Fig. 2E give R^2 values of 96% (for both the left and right sides); the fits in Fig. 2F gives R^2 values of 86 and 98% (left and right sides). The distribution of W_{eff} in all these experiments shows no significant outliers on the high end, meaning that the decay properties of the wave functions in Fig. 2, B to F, are not skewed by a small number of measurements.

Our results on disorder-enhanced transport call for a direct comparison between crystals and quasicrystals. We therefore simulate transport in triangular and QC lattices of the same mean lattice spacing. Figure 3A shows the simulated W_{eff} exiting the hexagonal lattice after propagating in it (z = 30 mm), as function of disorder strength. Clearly, for the hexagonal lattice, transport decreases monotonically with increasing disorder strength. In sharp contrast, for the QC lattice (Fig. 3B) increasing disorder first enhances transport, and only after reaching a pronounced peak transport begins to decline with increasing disorder. To examine the expansion rate of the beam, we follow W_{eff} while propagating through the QC (Fig. 3C) for different levels of disorder and calculate the derivative of log(W_{eff}) with respect to log(z) to deduce its characteristic exponent. Figure 3D reveals that the exponent of the expanding beam, for a wide range of disorder levels, is close to 0.5, indicating a diffusive-like expansion. Increasing the disorder past the level causing maximal transport (between 5 and 10% in Fig. 3B) shows that the exponent converges toward 0.5. By fitting W_{eff} versus z, the diffusion constants for 10, 30, 50, and 100% disorder are found to be 0.038, 0.029, 0.029, and 0.027 μm, respectively, giving mean free paths of 8.1, 6.3, 6.3, and 5.7 μm [derived as in (*3*)]. As clearly shown in Fig. 3C, the wave-packet widths greatly exceed these mean free paths, indicating that we are in the multiple-scattering regime. This fact, together with the characteristic exponent of 0.5, strongly suggests diffusive-like transport. We examine the log of the ensemble-averaged and azimuthally averaged beam intensities (over 100 realizations) in Fig. 3, E to H, as a function of the transverse radial coordinate, r. In these plots, for 0, 10, 30, and 50% disorder, respectively, we fit parabolas (Gaussian wave packets; i.e., diffusion) or lines (exponential wave packets; i.e., a signature of localization) only where the fit is highly appropriate (R^2 > 97%). We find that for 10% disorder (Fig. 3F), some features of the original QC remain; thus, parabolic and linear fits are not appropriate. For 30% disorder (Fig. 3G), a Gaussian wave packet is observed at z = 5 mm, whereas the wave packet shows the exponential tails signifying the start of localization by z = 20 mm. At 50% disorder (Fig. 3H), the wave packet quickly reaches exponential decay. As explained below, we use a narrow beam selected specifically to excite pseudogap states to demonstrate disorder-enhanced transport [unlike in (*3*) where a broader beam was used]. Consequently, the beam is a superposition of many eigenmodes, some of which have high energy and extremely large localization lengths, larger than the simulation box. Therefore, we do not observe the wave function coming to an absolute halt. It is well known that in two dimensions, some localization lengths can be extremely large and out of reach of any simulation. That said, the beam in Fig. 3, G and H, exhibits exponential decay (for $z \geq 10$ mm),

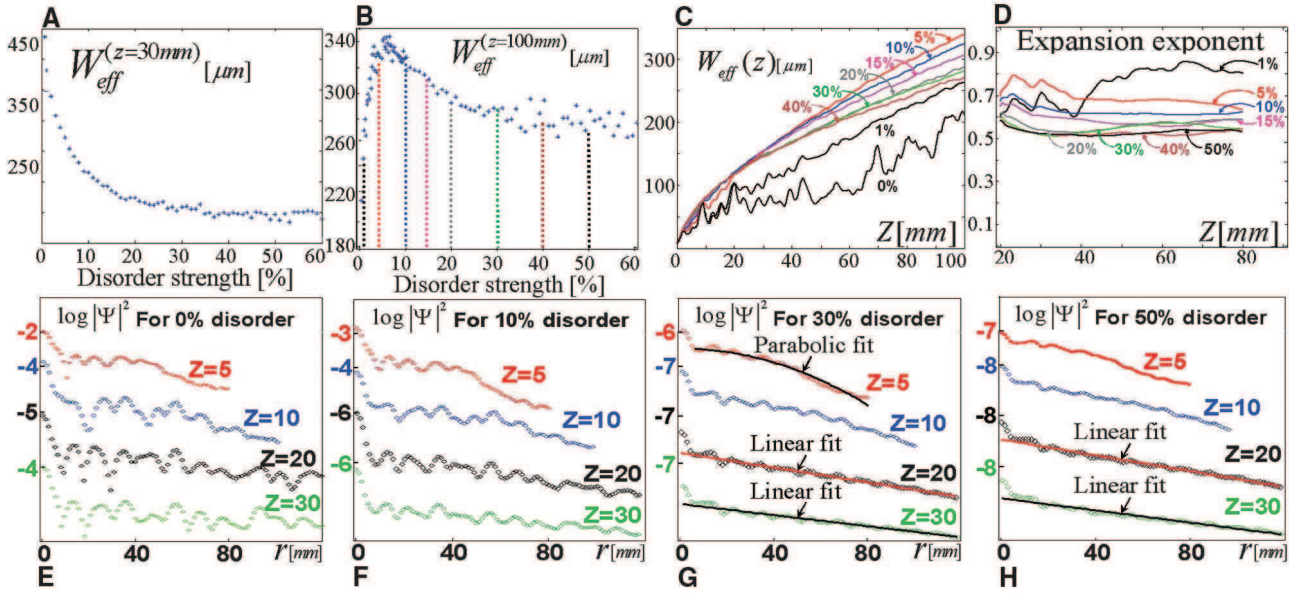

Fig. 3. Simulation results comparing transport through a hexagonal lattice and a QC for increasing disorder, showing disorder-enhanced and diffusive-like transport, as well as signatures of Anderson localization. (**A** and **B**) Ensemble-averaged beam width versus disorder strength for the hexagonal and QC lattices (same characteristic lattice spacing), showing disorder-enhanced transport for weak disorder (0 to 10%), then transport declines with further increase of disorder. (**C**) Beam width versus propagation distance in the QC for disorder levels indicated in (B). (**D**) The derivative with respect to log(z) of the log-log plot of (C); i.e., the characteristic expansion exponent. Convergence to 0.5 with increasing disorder indicates diffusive-like transport. (**E** to **H**) Logarithm of the ensemble- and azimuthally averaged wave function at 0, 10, 30, and 50% disorder, for various propagation distances. Parabolic fits indicate diffusive-like transport, and linear fits indicate the transition to Anderson localization for sufficiently large distances and disorder levels.

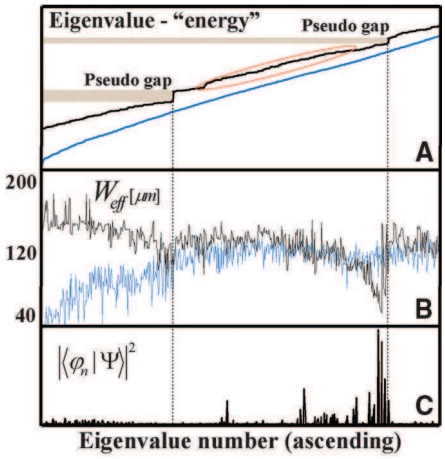

Fig. 4. Revealing the mechanism underlying disorder-enhanced transport in quasicrystals. (**A**) Band structure of a pure QC (black) and of a QC containing 20% disorder (blue). The fractured self-similar structure of the spectrum characteristic of a pure QC is smeared by the disorder, leading to a continuous density of states, which increases transport. The red oval denotes the fractal-like band. (**B**) W_{eff} of each eigenstate of a pure QC state (black) and in the QC containing 20% disorder (blue). Adding 20% disorder to a pure QC results in the broadening of all eigenfunctions associated with the vicinity of a large pseudogap (A). It is therefore expected that the expansion rate of a wave packet made up of such eigenfunctions will be higher in the disordered QC than in the pure QC. (**C**) Projection of a Gaussian wave packet (of Fig. 1A) on the eigenfunctions of the pure QC; φ_n represents the eigenfunctions. This wave packet, associated with the vicinity of a pseudogap, expands faster in a disordered QC, due to both the increase in the density of states (A) and to the broadening of the width, W_{eff}, of the eigenfunctions (B) in this region.

which is a clear signature that the wave packet is undergoing a transition to Anderson localization (*1*). The experimental and theoretical results displayed in Figs. 2 and 3 unequivocally show that disorder enhances transport in QCs; they demonstrate diffusive-like transport and show exponentially localized wave packets, a signature of the transition to Anderson localization.

These results raise the natural question: What is the underlying mechanism responsible for disorder-enhanced transport in QCs? Transport in atomic crystals is closely related to the density of states around the Fermi energy. In aperiodic systems, higher density of states is generally associated with broader eigenfunctions, which support higher transport. This is the case for potentials where the eigenmodes are localized (as in any potential containing disorder) or for critical states (as in QCs). To examine this point in our system, we solve Eq. 1 for a QC potential and find its eigenfunctions and eigenvalues β. Figure 4A shows a comparison between the band structure of a pure QC (black) and a QC containing 20% disorder (blue). The eigenvalues (energies) are presented in ascending order, because the notion of Brillouin zone does not exist for a QC. Nonetheless, there are regions (pseudogaps) in the band structure (gray in Fig. 4A) where the density of states is considerably lower. The band structure of the quasiperiodic potential is fractal-like; hence, higher-order pseudogaps exist on any scale (*12*). It is this fractured structure that is responsible for the low density of states, especially around pseudogaps, which in turn leads to highly localized states and thus to low conductivity/transport in QCs.

When disorder is introduced in a QC, the highly localized states near the pseudogap couple to one another, together forming eigenstates that are broader and less localized (at other energies, disorder acts to "smooth out" the fractal band structure, but the effect on transport is less pronounced). In other words, disorder mediates "hopping" between localized quasicrystalline eigenstates near the pseudogap (*30*). In turn, this coupling between localized states results in smoothing of the density of states, reducing the pseudogap until it altogether disappears (blue curve in Fig. 4A).

We calculate and plot W_{eff} of each of the eigenfunctions (Fig. 4B) for pure QC (black) and for the QC containing 20% disorder (blue). Going back to the plot of the eigenvalues (Fig. 4A), we find that the eigenstates near the two large pseudogaps tend to be more localized (Fig. 4B). At the same time, simple initial wave functions (e.g., Gaussian) are found to easily excite the localized eigenstates near the higher pseudogap, an experimentally indispensable condition. Figure 4B shows that adding 20% disorder to a pure QC results in the broadening of all eigenfunctions with energies in the vicinity of a large pseudogap. It is therefore expected that the expansion rate of a wave packet made up of such eigenfunctions will be higher in the disordered QC than in the pure QC. That is, the phenomenon of disorder-enhanced transport is expected to be most pronounced for wave packets associated with the pseudogaps in QCs. With this in mind, we analyze the wave packets launched in our simulations and experiments and examine their transport. Consider the Gaussian wave packet of Fig. 2A whose propagation displays enhanced transport in the disordered QC. Figure 4C displays the projection of this wave packet on the eigenfunctions of the pure QC. The underlying mechanism for disorder-enhanced transport in QCs is therefore due to the increase in the density of states near its pseudogaps. This explanation holds well for any launch point of a high 10-fold symmetry, which always excites mostly localized states from the vicinity of the pseudogap. Finally, we emphasize that the Fermi energy in atomic QCs resides in a pseudogap (similar to crystals where it resides in the gap), hence our initial wave packet represents conduction electrons residing in a k_BT-sized stripe (where k_B is the Boltzmann constant and T is temperature) around the Fermi energy.

This article was devoted to providing a direct experimental demonstration that transport in quasicrystals is enhanced by virtue of disorder, while displaying features associated with diffusion and localization. We studied this fundamental phenomenon and elucidated its origins, relating it to the basic properties of quasicrystalline media in the presence of disorder.

References and Notes

1. P. W. Anderson, *Phys. Rev.* **109**, 1492 (1958).
2. P. A. Lee, T. V. Ramakrishnan, *Rev. Mod. Phys.* **57**, 287 (1985).
3. T. Schwartz, G. Bartal, S. Fishman, M. Segev, *Nature* **446**, 52 (2007).
4. Y. Lahini *et al.*, *Phys. Rev. Lett.* **100**, 013906 (2008).
5. A. Szameit *et al.*, *Opt. Lett.* **35**, 1172 (2010).
6. D. S. Wiersma, P. Bartolini, A. Lagendijk, R. Righini, *Nature* **390**, 671 (1997).
7. A. A. Chabanov, M. Stoytchev, A. Z. Genack, *Nature* **404**, 850 (2000).
8. M. Störzer, P. Gross, C. M. Aegerter, G. Maret, *Phys. Rev. Lett.* **96**, 063904 (2006).
9. J. Billy *et al.*, *Nature* **453**, 891 (2008).
10. G. Roati *et al.*, *Nature* **453**, 895 (2008).
11. D. Shechtman, I. Blech, D. Gratias, J. W. Cahn, *Phys. Rev. Lett.* **53**, 1951 (1984).
12. D. Levine, P. J. Steinhardt, *Phys. Rev. Lett.* **53**, 2477 (1984).
13. T. Fujiwara, S. Yamamoto, G. Trambly de Laissardière, *Phys. Rev. Lett.* **71**, 4166 (1993).
14. D. Mayou, C. Berger, F. Cyrot-Lackmann, T. Klein, P. Lanco, *Phys. Rev. Lett.* **70**, 3915 (1993).
15. D. P. DiVicenzo, P. J. Steinhardt, Eds., *Quasicrystals, The State of the Art* (World Scientific, Singapore, 1991).
16. T. Fujiwara, M. Kohmoto, T. Tokihiro, *Phys. Rev. B* **40**, 7413 (1989).
17. T. Rieth, M. Schreiber, *Z. Phys. B* **104**, 99 (1997).
18. S. Roche, G. Tramblay de Lassardière, D. Mayou, *J. Math. Phys.* **38**, 1794 (1997).
19. F. Lederer *et al.*, *Phys. Rep.* **463**, 1 (2008).
20. B. Freedman *et al.*, *Nature* **440**, 1166 (2006).
21. B. Freedman, R. Lifshitz, J. W. Fleischer, M. Segev, *Nat. Mater.* **6**, 776 (2007).
22. Y. S. Chan, C. T. Chan, Z. Y. Liu, *Phys. Rev. Lett.* **80**, 956 (1998).
23. Y. Lahini *et al.*, *Phys. Rev. Lett.* **103**, 013901 (2009).
24. S. Roche, D. Mayou, *Phys. Rev. Lett.* **79**, 2518 (1997).
25. H. De Raedt, A. Lagendijk, P. de Vries, *Phys. Rev. Lett.* **62**, 47 (1989).
26. J. W. Fleischer, M. Segev, N. K. Efremidis, D. N. Christodoulides, *Nature* **422**, 147 (2003).
27. For details, see the supporting material on *Science* Online.
28. M. Segev, G. C. Valley, B. Crosignani, P. DiPorto, A. Yariv, *Phys. Rev. Lett.* **73**, 3211 (1994).
29. For each realization of disorder, the confinement of the beam at the output plane is quantified by the inverse participation ratio $P \equiv \left[\int I(x,y,L)^2 dxdy\right] / \left[\int I(x,y,L)dxdy\right]^2$ (where I is the intensity and L is the propagation distance), having units of inverse-area and an average effective width $W_{eff} = \langle P \rangle^{-1/2}$; the averaging is over multiple realizations of the disorder (same statistics).
30. We emphasize that the disorder-enhanced transport in QCs observed here is fundamentally different from transport effects associated with the Urbach tail. See detailed discussion in (*27*).

Acknowledgments: This work was supported by an Advanced Grant from the European Research Council, the Israel Ministry of Science, the German-Israeli Foundation, and the Israel Science Foundation. M.R. gratefully acknowledges the generous support of an Azrieli Postdoctoral Fellowship. All authors thank S. Fishman, B. Shapiro, and Y. Krivolapov for useful discussions.

Supporting Online Material

www.sciencemag.org/cgi/content/full/science.1202977/DC1
Materials and Methods
SOM Text
Fig. S1
References

18 January 2011; accepted 28 April 2011
Published online 12 May 2011;
10.1126/science.1202977

Disorder-Enhanced Transport in Photonic Quasicrystals

L. Levi, M. Rechtsman, B. Freedman, T. Schwartz, O. Manela and M. Segev

Physics Department and Solid State Institute, Technion, Haifa 32000, Israel

Supporting Online Material

Section 1: Experimental Methods

We work with photonic lattices (1), in the transverse localization scheme (2), which is described by the paraxial wave equation (Eq. 1) for monochromatic light, namely the Schrödinger equation. Construction of the quasicrystal (QC) photonic lattice is based on the optical induction technique (3), which has been extensively used to study a variety of nonlinear wave phenomena in photonic lattices (4,5). The specific technique used here utilizes the photorefractive screening effect (6) inside a 10*mm*-long SBN:60 crystal, in which separation of optically-excited charges (electrons) creates a varying electric space-charge field, which in turn induces a local change in the refractive index via the electro-optic effect. The end result is the creation of a spatially-dependent refractive index profile from an optical interference pattern (1,3,4).

In the experiments described here, we aim to induce a refractive index structure which is uniform (non-varying) in the propagation direction, z, and quasi-ordered in the other two (transverse), with random fluctuations superimposed on it. The experimental setting for making the QC with the controlled disorder is shown in the figure below. The QC is induced by five plane-waves (Gaussian beam with a diameter of 1cm) at a wavelength of 514nm, which share a common z-axis, and are arranged such that the projection of the *k*-vectors of these lattice-forming waves on the x-y plane reside on a ring (whose center is on the z-axis) and have a 72° angle between one another. These beams interfere to produce a ten-fold Penrose tilling interference pattern (Fig 1A) with a typical spacing between speckles of ~12μ*m*. The z-independent disorder is constructed by interfering plane waves with random amplitude and phase, with all waves residing on the ring described above. Experimentally, to make the disorder propagation-invariant, we pass a laser beam through a conical lens, which creates a narrow ring of light at the Fourier plane of a 4f system, where a diffuser is placed at its center. When the thickness of the ring is considerably narrower than the typical size of a scatterer upon the diffuser, the speckled pattern formed at the output of the 4f system does not vary while propagating even for large distances. The diffuser is

rotated automatically, in discrete steps, such that the laser beam passes through a different location on the diffuser in each step. This generates a new speckled pattern in each step, and introduces a different realization of the disordered lattice, enabling us to generate an ensemble of realizations.

Overall, the waves inducing the QC and the waves inducing the disorder are coherently overlaid on the same ring at the Fourier plane (k_x,k_y-space), such that they all accumulate phase at the same rate while propagating along the z-axis. That is, all the plane waves making up the lattice and perturbations now have the same projection (longitudinal momentum) on the propagation axis, z . This results in a 2D transverse interference pattern that does not depend on z (for a distance larger than the 10mm of propagation length in our the SBN:60 crystal, where the experiment is conducted).

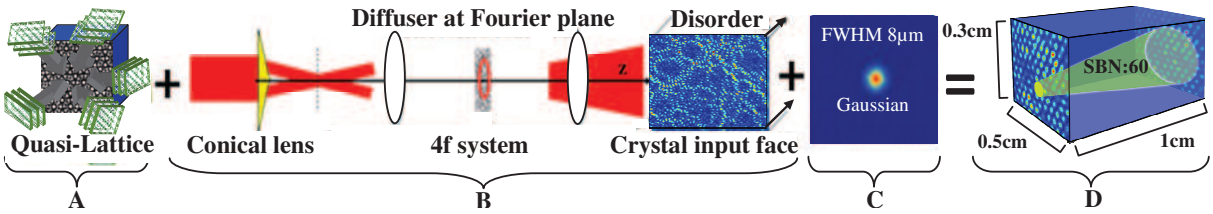

Experimental scheme for transverse localization in photonic quasicrystals containing disorder. The interference of five plane waves (A) creates a Penrose Quasi-Crystal lattice. Disorder is created by passing a wide beam through a conical lens, and then placing a diffuser at the focal plane located in the middle of the 4f system (B). Disorder and lattice are then both coherently added and imaged to the input facet of the photosensitive crystal within which they induce the photonic quasicrystal. The probe beam (C) is launched at the input plane of the disordered QC, and monitored at the output plane (D). Controlling the strength of the disorder is done by changing the ratio between the total intensity of the beam inducing the disorder, and the total intensity of the beams creating the underlying lattice.

In order to create modulations in the index of refraction inside the SBN:60 via the photorefractive screening effect (6), we apply a bias electric field of ~3000*Volt/cm* which yields an index contrast of ~ 4-5 10^{-4}. To set the degree of saturation of the photorefractive screening nonlinearity, we add a uniform, ordinarily polarized (normal to the c-axis of the SBN crystal) optical beam of the same wavelength, which serves as the background illumination (6). This beam is made to be spatially-incoherent in order to avoid its breakup by possible modulation instability (9,10). The local refractive index profile is a function of the ratio between the local

intensity pattern (lattice + disorder) and the intensity of the uniform background beam. In the current experiments, we operate the effect at deep saturation: intensity ratio 4 (background beam 4 times weaker than the interference pattern forming the lattice + disorder). It is necessary for this ratio to be significantly greater than unity in order to generate the high harmonics in the QC diffraction pattern (7,8), as they appear in the diffraction pattern of atomic QCs.

Determining the relative strength of the disorder is done by controlling the intensity of the waves inducing the disorder, relative to the total intensity of the interference pattern inducing the QC lattice + disorder, namely, the ratio between the power contained in the spatial spectrum of the disorder relative to the total power contained in the lattice + disorder. All of these beams inducing the disordered lattice are ordinarily polarized (normal to the c-axis of the SBN:60 crystal), and hence propagate linearly in the medium, meaning that they induce the photonic lattice, but do not respond to it (3,4).

The probe beam is a weak narrow Gaussian beam of 9μm Full-Width-Half-Maximum, of the same wavelength. Keeping in mind that enhanced transport occurs for wavepackets located around a specific pseudogap (second psedogap in Fig 4c), we chose the width of the probe beam by numerically evaluating its projection upon the eigenmodes of the QC, searching for a width that is both experimentally accessible and gives a sufficient projection upon the second pseudogap. The probe beam is made extraordinarily polarized (parallel to the c-axis of the SBN:60 crystal), such that it responds to the refractive index structure induced be the lattice-forming beams. The intensity of the probe beam is set to be sufficiently weak, having a negligible contribution to the refractive index, hence propagating linearly through the medium.

Finally, after each measurement and before inducing a new disordered lattice, we illuminate the photorefractive crystal with a uniform, intense, light beam (from a white light source), assuring there are no traces left from the refractive index distribution induced in a previous experiment.

Section 2: Discussion on disorder-enhanced transport and the Urbach tail

It is important to emphasize the distinction between the type of disorder-enhanced transport we observe in QCs, and the leaking of eigenstates into the band gap of a periodic system as a result of disorder (the Urbach tail). We highlight the difference between these two mechanisms here

by examining the Urbach tail effects in photonic crystals. Consider a finite photonic crystal with a complete band gap, and light incident upon it, with energy (or frequency) in the band gap. Since there are no propagating modes in the finite photonic crystal, the incident light will be entirely reflected. However, if disorder is introduced into the system, eigenstates penetrate into the gap and will allow greater transmission across the sample. This is an example of disorder-induced transport by virtue of the Urbach tail, but it is entirely different from the effect we observe in the present work, as we explain below.

In the present work, we use an effectively infinite system that is z-invariant (or, in the language of quantum mechanics, the potential is time-invariant). The eigenmodes of our quasicrystalline system form a complete set. Hence, when we launch a wavepacket we may only excite the bulk modes present in the system, including highly localized fractal QC modes, as discussed in the article. Since these modes become delocalized as a result of disorder, we observe disorder-enhanced transport (or delocalization). This would be absolutely impossible in a periodic system, since there are no bulk modes in the band gap to excite in the first place, by the very definition of a band gap. In stark contrast to the QC, any initial wavefunction in a periodic system would undergo localization as a result of disorder, regardless of the Urbach tail.

Section 3: Discussion of correlations in the disorder

While there are correlations in the disorder (as there will be with any speckle pattern), these correlations have little qualitative effect on localization properties in our photonic system. Recall that the potential is generated in the saturated regime, as described in first section above, hence the transverse momentum of the disorder spans much beyond the transverse momentum of the waves inducing the disorder, as well as the transverse momentum of the probe beam used to test localization. As such, the disorder can scatter at high wavenumbers. Physically (in the experiments), the momentum bandwidth of the disorder induced by the speckled beam is finite (6): the highest wavenumbers that can be induced in a photorefractive crystal are on the order of the 2π/Debye screening length. But this length scale is ~0.5μm in our SBN crystal, at least 20 times smaller than both the mean lattice constant and our initial beam width. That is, our system supports disorder with a maximum momentum span that is 20 times larger than the momentum

of our initial wavepacket. Consequently, the `effective mobility edge' resulting from correlations (11,12) has a negligible effect in our system.

1. Schwartz, T., Bartal, G., Fishman, S. & Segev, M. Transport and Anderson localization in disordered two-dimensional photonic lattices. *Nature* **446**, 7131 52-55 (2007).
2. De Raedt, H., Lagendijk, A. & de Vries, P. Transverse localization of light. *Phys. Rev. Lett.* **62**, 47-50 (1988).
3. Efremidis, N.K., Sears, S.M., Christodoulides, D.N., Fleischer, J.W. & Segev, M. Discrete solitons in photorefractive optically-induced photonic lattices. *Phys. Rev. E* **66**, 046602 (2002).
4. Fleischer, J.W., Segev, M., Efremidis, N.K & Christodoulides, D.N. Observation of two-dimensional discrete solitons in optically induced nonlinear photonic lattices. *Nature* **422**, 147-150 (2003)
5. Lederer, F. et. al., Discrete solitons in optics. *Phys. Rep.* **463**, 1-126 (2008).
6. Segev, M., Valley, G. C., Crosignani, B., DiPorto, P. & Yariv A. Steady-State Spatial Screening Solitons in Photorefractive Materials with External Applied Field *Phys. Rev. Lett.* **73**, 3211–3214 (1994)
7. Freedman, B. et. al., Wave and defect dynamics in nonlinear photonic quasicrystals. *Nature* **440**, 1166-1169 (2006)
8. Freedman, B., Lifshitz, R., Fleischer, J.W. & Segev, M. Phason dynamics in nonlinear photonic quasicrystals. *Nature Materials* **6**, 776-781 (2007)
9. Soljacic, M., Segev, M., Coskun, T., Christodoulides, D.N. & Vishwanath A. Modulation instability of incoherent beams in noninstantaneous nonlinear media. *Phys. Rev. Lett.* **84**, 467-470 (2000)
10. Kip, D., Soljacic, M., Segev, M., Eugenieva, E. & Christodoulides, D.N. Modulation instability and pattern formation in spatially incoherent light beams. *Science* **290**, 495-498 (2000)
11. Billy, J. et. al., Direct observation of Anderson localization of matter waves in a controlled disorder. *Nature* **453**, 891-894 (2008).
12. Sanchez-Palencia, L. et al.. Anderson localization of expanding Bose-Einstein condensates in random potential. *Phys. Rev. Lett.* **98**, 210401 (2007)